Linewidth Narrowing with Ultimate Confinement of an Alkali Multipole Plasmon by Modifying Surface Electronic Wave Functions with Two-Dimensional Materials

Shunsuke Tanaka,[1] Tatsuya Yoshida,[1] Kazuya Watanabe,[1,*] Yoshiyasu Matsumoto,[1]
Tomokazu Yasuike,[2,3,†] Marin Petrović,[4] and Marko Kralj[4]

[1]Department of Chemistry, Graduate School of Science, Kyoto University, Kyoto 606-8502, Japan
[2]Department of Liberal Arts, The Open University of Japan, Chiba 261-8586, Japan
[3]Elements Strategy Initiative for Catalysts and Batteries, Kyoto University, Kyoto 615-8520, Japan
[4]Center of Excellence for Advanced Materials and Sensing Devices, Institute of Physics, Bijenička 46, 10000 Zagreb, Croatia

This work demonstrates significant line narrowing of a surface multipole plasmon (MP) by modifying the surface electronic wave function with two-dimensional materials (2DMs): graphene and hexagonal boron nitride. This is found in an optical reflectivity of alkali atoms (Cs or K) on an Ir(111) surface covered with the 2DMs. The reduction in reflectivity induced by deposition of the alkali atoms becomes as large as 20% at ~2 eV, which is ascribed to a MP of a composite of alkali/2DM/alkali/Ir multilayer structure. The linewidth of the MP band becomes as narrow as 0.2 eV by the presence of the 2DM between the two alkali layers. A numerical simulation by time-dependent density functional theory with a jellium model reveals that the density of states of the surface localized state is sharpened remarkably by the 2DMs that decouple the outermost alkali layer from the Ir bulk. Consequently, a local field enhancement of an order of 10^5 is achieved by ultimate confinement of the MP within the outermost alkali layer. This work leads to a novel strategy for reducing plasmon dissipation in an atomically thin layer via atomic scale modification of surface structure.

There has been a growing interest in nanophotonics in atomically thin two-dimensional materials (2DMs) because of their potential for energy harvesting, optoelectronics, and biomedical technologies [1–3]. The key concept behind these wide-ranging applications is plasmonic excitation in reduced dimension, which enables strong field confinements that support various novel functionalities.

While the recent progress in nanoscale photonics is rooted in early studies on the surface plasmon supported at the metal-dielectric interfaces [4,5], much less recognized is that the same interface can also support a multipole plasmon (MP) [6–8] that exhibits an induced charge density with a dipole character along the interface normal. An adequate theoretical description of the MP requires quantum mechanical treatment of the electron density profile at the interface, and the MP served as an early test bed for nonlocal descriptions of the interfaces [6]. Contrary to its monopole counterpart, the dipole character of MPs allows a direct coupling with a free space electromagnetic wave without additional momentum compensation: this is a significant advantage in photonics application. Moreover, a MP exhibits an almost "flat" dispersion curve [8], implying that a giant field enhancement can be realized by a very small group velocity of the excitation [9,10].

Historically, an unambiguous identification of MPs was demonstrated for thin metallic overlayer films deposited on a flat metal substrate. Pronounced responses of MPs have been observed only for films of alkali metals and silver thicker than several monolayers [11,12]. On the other hand, an atomically thin overlayer does not support a well-developed MP and only exhibits an absorption feature broader than 1 eV [13]. This is due to an insufficient electron density and a strong coupling with the substrate in the single atomic layer [6,8,14]. Consequently, it is believed to be tremendously difficult to confine a MP in a single atomic layer. Therefore, establishing a methodology to achieve the pronounced MP response with downsizing of the overlayer thickness to a monolayer level is a challenge worth pursuing.

Contrary to the previous belief, here we demonstrate that single layer alkali atoms can support strong and sharp MP responses by tailoring of the interface wave function. This becomes possible by fabricating a multilayer structure in which a graphene (Gr) or hexagonal boron nitride (h-BN) is sandwiched by the alkali atom layers on an Ir(111) substrate. The outermost single alkali layer exhibits an absorption linewidth of 0.2 eV in the visible frequency region: this is significantly reduced from the MP bandwidth of the corresponding bulk alkali metals [8]. In addition, the absorption magnitude reaches ~20%, far exceeding known single layer absorbance by other 2D materials (2% for graphene; 10% for MoS_2) [1]. This remarkable feature is successfully simulated by time-dependent density functional theory (TDDFT) calculations using a jellium

model [6]; the analysis reveals that the line narrowing originates in the decoupling of the surface localized state involved in the plasmon from the bulk with the help of the 2DMs. It turns out that the strong modification of the MP response in the multilayer structure clearly manifests the quantum effect on the surface plasmon response in which a change in the electron density profile at the interface plays a crucial role [15–19].

Experiments were carried out in an UHV chamber (base pressure $< 4 \times 10^{-8}$ Pa) (see Supplemental Material [20], Sec. I) [33,34]. An Ir(111) single crystal was cleaned by cycles of Ar^+ sputtering followed by annealing at 1470 K, showing a sharp (1×1) low energy electron diffraction (LEED) pattern (see Ref. [20], Sec. I for details). Monolayer (ML) Gr was prepared by decomposition of ethylene in temperature programmed growth followed by chemical vapor deposition (CVD) [35], and monolayer h-BN was formed by CVD with ammonia borane [36]. The quality and uniformity of the 2DMs were confirmed by moiré superstructures in LEED (Fig. S2 in Supplemental Material [20]).

Alkali (Cs or K) atoms were deposited from a well degassed source (SAES Getters) on the Ir(111) surface covered with either Gr or h-BN. After the complete intercalation of alkali atoms between the 2DM and Ir substrate, the second layer grows on top of the 2DM [21,22]. This structural engineering was used for strong electron doping of graphene to explore the warping of its Fermi surface towards doping levels close to the van Hove singularity [37]. The optical reflectivity change was measured *in situ* during the alkali deposition process (see Supplemental Material [20], Sec. I for the details). The amount of the alkali atoms intercalated between the 2DM and the Ir substrate and adsorbed on top of the 2DM is estimated by the LEED observation and by ultraviolet photoemission spectroscopy (see Supplemental Material [20], Secs. I and II).

Figures 1(a) and 1(b) show typical reflectance-loss spectra for *p*-polarized light $\Delta R_p(\theta) = 1 - I(\theta)/I(0)$ during the Cs deposition at 300 K on (a) clean Ir(111) and (b) Gr-covered Ir(111), respectively, where $I(\theta)$ is the reflection spectrum at a Cs coverage θ (ML). In Fig. 1(a), a broad increase in ΔR_p covering the whole observation energy window grows with θ. We note that Cs deposition saturates at 1 ML on Ir at 300 K and that the broad spectrum is consistent with the response of monolayer Cs in literature [13]. In contrast, when Cs is deposited on a Gr covered Ir (111) surface, a strong reflectance-loss peak grows up to $\sim 20\%$ and a line width of ~ 0.2 eV (see Supplemental Material [20], Sec. III) at 2.0–2.3 eV, whose peak energy is blueshifted with θ [Fig. 1(b)]. We note that because the transmittance of light is negligible, the reflectance loss ΔR_p corresponds to the absorption induced by the alkali deposition. The coverage of the Cs overlayer that gives the sharp absorption was estimated to be 0.6–0.8 ML on top of a Gr/Ir(111) that is fully intercalated with Cs. Therefore, a
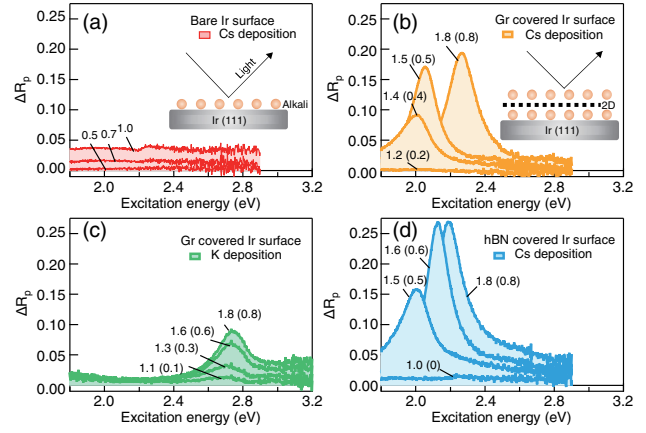

FIG. 1. Reflectivity changes of *p*-polarized light $\Delta R_p(\theta)$ as a function of alkali coverage θ (ML). (a) Clean Ir surface with Cs deposition at 300 K. (b) Gr covered Ir surface with Cs deposition at 300 K. (c) Gr covered Ir surface with K deposition at 300 K. (d) h-BN covered Ir surface with Cs deposition at 120 K. The insets in (a) and (b) show schematic illustration of the corresponding sample surface. The numbers in figures indicate the alkali coverage θ. Note that at $\theta > 1$ ML for Gr or h-BN covered surfaces, the 2DM is fully intercalated with the alkali atoms and additional alkali atoms adsorb on top of the 2DM. The numbers in parentheses indicate the alkali coverage adsorbed on top of the 2DM.

structure of Cs(0.6–0.8 ML)/Gr/Cs(1 ML)/Ir(111), in which the graphene is sandwiched by the Cs layers, is essential for the remarkable sharp absorption to appear [see inset of Fig. 1(b)]. The ΔR_p spectrum of the intercalated Gr/Ir without the top layer Cs only shows a flat spectral response (see Supplemental Material [20], Sec. II): the intercalated Cs shares its electron with both graphene and Ir substrate [21], losing the electron density to sustain the MP [see Fig. 2(d) and discussion below]. Adding the top layer Cs induces the MP response with considerable line narrowing. The incident angle dependence of the giant narrow band indicates that the band intensity follows the electric field strength normal to the surface: this is the known character of a MP (see Supplemental Material [20], Sec. V for details).

A similar narrow band response is observed also for K deposition. Figure 1(c) shows reflectance-loss spectra observed for K deposition on a Gr covered Ir(111). The peak energy is blueshifted by ~ 0.5 eV from the case with the Cs deposition. The ratio of the peak energy between the two alkali atoms (Cs and K) coincides with the ratio of their bulk plasma frequencies [8], supporting that the peak is caused by the alkali adsorbates. We note that the MP response energies in the present work [2.3 (Cs) and 2.9 eV (K)] are fully in agreement with the universal property of the MP energy $\omega_{MP} \approx 0.8 \omega_{BP}$ [8], where bulk plasmon energies ω_{BP} are 2.9 (Cs) and 3.8 eV (K) [8].

Further information on the role of the 2DMs can be obtained by replacing the Gr with h-BN. Figure 1(d) shows

the reflectivity change with Cs deposition on a h-BN covered Ir(111), which again gives a sharp reflectance loss. Because the electronic structure of Gr is quite different from that of h-BN, the observation of a common feature irrespective of the nature of the 2DMs supports our claims that the sharp band is due to the MP of alkali layers. Consequently, the question arises as to what is the role of the 2DMs in the peculiar optical responses.

In order to obtain further insights, we carried out TDDFT simulations by using a jellium model. All the calculations were performed with the prescription given by Liebsch [6] (see Sec. VII in Supplemental Material [20] for computational details).

Our particular concern is the perpendicular component of Feibelman's d parameter [23], $d_\perp$, which is given by a centroid of the surface charge induced by a uniform electric field normal to the surface with frequency ω:

$$d_\perp(\omega) = \frac{\int dz z \delta n(z,\omega)}{\int dz \delta n(z,\omega)}, \qquad (1)$$

where $\delta n(z,\omega)$ is the induced charge density and z is the distance along the surface normal. The imaginary part of $d_\perp$ is directly related to the reflectance loss at the surface, $\Delta R_p \propto \mathrm{Im} d_\perp$ (see Supplemental Material [20], Sec. VI).

The calculated $\mathrm{Im} d_\perp$ for the model simulating 1.0 ML Cs on a clean Ir (without Gr) is shown in Fig. 2(a), which exhibits a broad band (FWHM ~ 0.7 eV) qualitatively explaining the experimentally observed reflectance-loss spectrum [Fig. 1(a)]. The calculation shows the increase in the absorption with increasing the Cs coverage up to 2 ML; that also reproduces the observed spectrum (see Sec. IV in the Supplemental Material [20]). Figure 2(b) shows the induced charge density profiles at the spectral peak energy, exhibiting a dipolar character along the surface normal agreeing with the MP response in literature [6].

Having confirmed the validity of the current theoretical approach on Cs/Ir(111), we simulate the spectra of the multilayer structure with the alkali and 2DMs (see Sec. VII in the Supplemental Material [20] for the calculation details). The presence of the Gr layer drastically affects the spectral response of $\mathrm{Im} d_\perp$ as plotted in Fig. 2(c). The peak width of the absorption is reduced down to ~ 0.09 eV, which is qualitatively consistent with the observation. The overestimated peak energies are caused by a well-known limitation of the jellium model [13], and are not essential for the present study. The induced electron density profiles at the peak energies shown in Fig. 2(d) exhibit dipolar shapes mostly in the Cs top layer, indicating the common MP character irrespective with the coverage and alkali/2D species. Note that, in Fig. 2(d), the intercalated alkali layers only show negligible contributions to the induced densities while the remarkable changes in the density are concentrated in the outermost alkali layers on top of the 2DMs. Figure 2(c) demonstrates the blueshifts of the peak energy
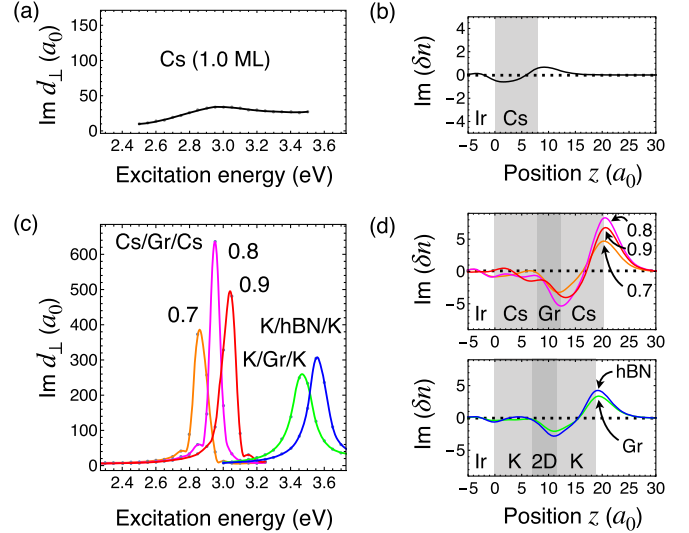

FIG. 2. (a) Computed $\mathrm{Im} d_\perp(\omega)$ spectrum for Cs (1 ML) on Ir. (b) $\mathrm{Im}[\delta n(z,\omega)]$ of Cs on Ir for ω at the peak of the spectrum in (a). The gray region indicates Cs layer in the jellium model. (c) Computed $\mathrm{Im} d_\perp(\omega)$ spectra for Cs/Gr/Cs/Ir (orange, magenta, and red), K/Gr/K/Ir (green) and K/h-BN/K/Ir (blue). The coverage of the outermost alkali is 0.7 (orange), 0.8 (magenta), and 0.9 ML (red) for Cs, and 0.9 ML for K. (d) $\mathrm{Im}[\delta n(z,\omega)]$ corresponding to (c) for ω at each peak of Cs/Gr/Cs/Ir (top), K/Gr/K/Ir and K/h-BN/K/Ir (bottom). The light (dark) gray region indicates alkali (2DM) layers. The color code corresponds to that in (c).

with increasing the alkali coverage. The strong peak appears persistently when Gr is replaced with h-BN. Consequently, our theoretical modeling captures all the experimental features of the optical response of the multilayer structure. The large induced densities in Fig. 2(d) should lead to strong induced electric fields $E(z)$ at the outermost alkali layer. Indeed, the maximum enhancement factor of the induced field relative to the incident one E_0 for Cs(0.8 ML)/Gr/Cs/Ir(111), $|E(z)/E_0|^2$, is estimated to be 3.3×10^5. This is much higher than the reported values of $\sim 10^2$ for a surface plasmon polariton on a silver surface [38] and sphere [39], indicating that the remarkable local field enhancement occurs in the alkali layer thanks to the confinement in the atomically thin region.

In order to understand the physical origin of the sharp and intense absorption peaks induced by the 2DMs, it is useful to decompose $\mathrm{Im} d_\perp(\omega)$ into contributions from the individual excitations by using the one-particle spectral representation of the involved Green's function. In the scattering formalism given by Liebsch, the Green's function has the form of the energy integral and is not suitable for extracting physical insight in a compact manner. We thus employ the complex-scaling scattering theory [24] (see Supplemental Material [20], Sec. VIII for additional details) to obtain a compact discrete representation. In this framework, the scattering continuum and embedded discrete states in a semi-infinite bulk are approximated

TABLE I.   Calculated values of $\mathrm{Im}d_\perp^{m\to j}(\omega_p)$ for $\omega_p = 3.05$ eV for the transitions between occupied ($m = 1$–4) and virtual ($j = 1$–3) orbitals for the Cs(1.0 ML)/Ir and Cs(0.9 ML)/Gr/ Cs(1.0 ML)/Ir systems. The above value of ω_p corresponds to the peak energy of the transitions depicted in Fig. 2. See Fig. 3 for the density of states and wave function of each orbital.

Cs/Ir		
$j = 1$	$j = 2$	$j = 3$
1.925	3.565	5.460
5.779	7.557	8.395
3.761	3.134	1.099
2.077	0.301	0.000

where the rows are $m=1$, $m=2$, $m=3$, $m=4$

Cs/Gr/Cs/Ir		
$j = 1$	$j = 2$	$j = 3$
162.830	89.888	47.641
163.480	72.828	5.127
−3.428	−10.248	−8.197
−38.655	−21.364	−3.996

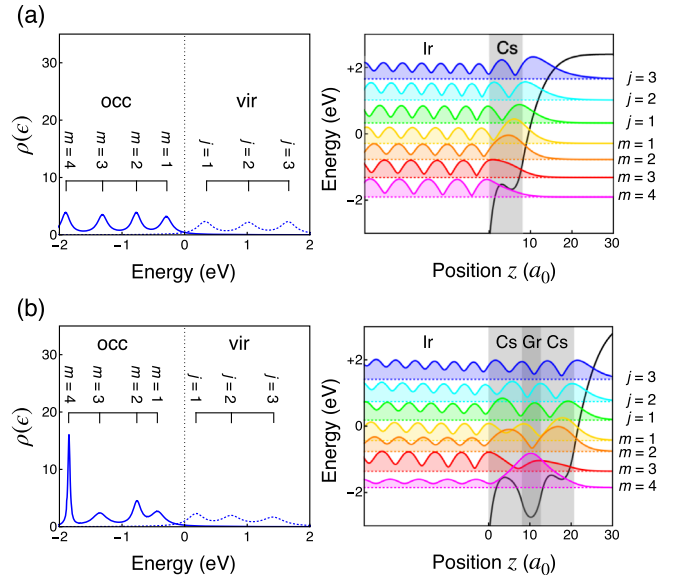where the rows are $m=1$, $m=2$, $m=3$, $m=4$

FIG. 3.   (Left) the density of states for the one-particle states near the Fermi level. Solid (dotted) curves show the occupied (virtual) states. (Right) (colored curves) the modulus square of the wave functions of the one-particle states superposed with electronic potentials plotted with black. The offsets of each wave function correspond to the energy of the one-particle states $\mathrm{Re}[\epsilon_{m,j}]$. The gray shaded regions indicate the Cs and Gr layers. Indices m (occupied) and j (virtual) correspond to those in Table I. The origin of the energy is set to the Fermi level. (a) Cs (1.0 ML)/Ir and (b) Cs(0.9 ML)/Gr/Cs(1.0 ML)/Ir.

appropriately with discrete one-particle states (orbitals) having complex-valued energies. This enables us to decompose $\mathrm{Im}d_\perp(\omega)$ into a summation of the individual excitations from an occupied orbital ψ_m to a virtual unoccupied one ψ_j: $\mathrm{Im}d_\perp(\omega) = \sum_{m,j}\mathrm{Im}d_\perp^{m\to j}(\omega)$.

Among the one-particle eigenstates of the complex-scaled Hamiltonian, a few states localized on the surface region possess relatively small imaginary parts of the energy, indicating that they are decoupled from the bulk. The spatially localized and long-lived states embedded in a continuum spectrum are generally called "resonance states." In the present systems, such states significantly contribute to the surface optical response $\mathrm{Im}d_\perp$ and we focus on their contributions $\mathrm{Im}d_\perp^{m\to j}(\omega)$ to the transitions shown in Fig. 2. Hereafter, these resonances are referred to as "adlayer resonance states."

Our analysis shows that the prominent peak in Fig. 2 is a superposition of many individual excitations among several orbitals reflecting the collectiveness of the plasmonic transition [25] (see Supplemental Material [20], Sec. VIII). In addition, the prominent components in $\mathrm{Im}d_\perp^{m\to j}$ are concentrated in transitions between the occupied and virtual orbitals located within ± 2 eV from the Fermi level.

The spectral contributions of these most prominent transitions for $1{\le}m{\le}4$ and $1{\le}j{\le}3$, are given in Table I, where the orbitals are numbered in order of $|\mathrm{Re}[\epsilon_{m,j}]|$ from the Fermi level. It is clear that the magnitude of $\mathrm{Im}d_\perp^{m\to j}$ is significantly larger for the Cs/Gr/Cs/Ir than the Cs/Ir, causing the giant absorption in the former multilayer structure.

The origin of the band narrowing of the MP is revealed by inspecting the density of states (DOS) and the wave functions of the orbitals. These are shown in Figs. 3(a) and 3(b) for Cs(1.0 ML)/Ir and Cs(0.9 ML)/Gr/Cs(1.0 ML)/Ir, respectively. We note that the wave functions with $m = 4$ for Cs/Ir and with $m = 3$ for Cs/Gr/Cs/Ir exhibit larger amplitudes in bulk than at the adlayer regions and are not assigned to adlayer resonances but to discretized continua. Therefore, the orbitals categorized to the occupied adlayer resonances are those with indices of $m = 1, 2, 3$ for Cs/Ir and $m = 1, 2, 4$ for Cs/Gr/Cs/Ir.

The most striking feature in the DOS plots is the large difference in the band width of the lowest occupied adlayer resonance: the width becomes significantly narrowed in $m = 4$ of Cs/Gr/Cs/Ir [Fig. 3(b), left] than that in $m = 3$ of Cs/Ir [Fig. 3(a), left]. Note that the energy widths of the occupied and virtual adlayer resonances determine the rate of dissipation from the individual surface excitation to the hole and particle states in the bulk, respectively. Therefore, the significant narrowing in the occupied adlayer resonances in Cs/Gr/Cs/Ir is crucial for the bandwidth reduction of the plasmonic excitation.

The DOS sharpening of the occupied adlayer resonace is clearly understood by examining the corresponding wave functions and the potential supporting them. The potential for the surface region of Cs/Ir is very shallow and only supports short-lived resonances with wave functions extending into the bulk [the right panel in Fig. 3(a)].

In contrast, the surface potential of Cs/Gr/Cs/Ir has a deep well originating from Gr and strongly supports a well-localized resonance state [$m = 4$, the magenta curve in the right panel in Fig. 3(b)]. This resonance state is well decoupled from the bulk and exhibits a very sharp DOS in the left panel in Fig. 3(b) ($m = 4$). Therefore, the origin of the band narrowing with the 2DMs is ascribable to the decoupling of the adlayer resonances from the bulk by the trapping of them into the 2DM potentials supporting their π bands.

The mechanism of the significant enhancement in $\mathrm{Im}d_\perp^{m \to j}$ for Cs/Gr/Cs/Ir can be rationalized by considering the shape of the wave functions of the adlayer resonances: the first and second occupied adlayer resonances ($m = 1$, 2) of Cs/Gr/Cs/Ir [the yellow and orange curve wave functions in Fig. 3(b) right] are orthogonal to the lowest one ($m = 4$, magenta) localized at the Gr layer. Thus, they have nodes at the Gr-layer region leading to more localized charge densities at Gr/outer-Cs interface than without Gr. Consequently, a strong charge transfer from Gr/outer-Cs to outer-Cs/Gr interfaces occurs [as depicted in Fig. 2(d)], leading to the significant enhancement in $\mathrm{Im}d_\perp$. We note that a similar mechanism operates also for h-BN: while the electronic structures of Gr and h-BN are quite different around the Fermi level, their π band structures at K and M points in the Brillouin zone located at 2–3 eV below the Fermi level are similar to each other. Because these π bands are energetically close to the Cs $6sp$ bands, modifications of the wave function discussed above become possible.

In conclusion, we have demonstrated the ultimate downsizing of the MP supporting layer by fabricating the 2DM sandwiched by atomically thin alkali layers. Our theoretical analysis showed that the 2DMs effectively localize the adlayer resonances at the surface region and suppress the plasmon dissipation, giving rise to the line narrowing and the local field enhancement. This novel strategy for tailoring the plasmon response by atomic scale structural control will pave the way for taming the dynamical properties of surface plasmons [40,41]. In addition, the theoretical approach presented in this work would be helpful in future prediction and analysis of the quantum effects in surface plasmons in which surface atomic structure is systematically varied.

[*]kw@kuchem.kyoto-u.ac.jp
[†]yasuike@ouj.ac.jp

[1] F. Xia, H. Wang, D. Xiao, M. Dubey, and A. Ramasubramaniam, Nat. Photonics **8**, 899 (2014).

[2] P. A. D. Gonçalves, N. Stenger, J. D. Cox, N. A. Mortensen, and S. Xiao, Adv. Opt. Mater. **8**, 1901473 (2020).

[3] T. Low, A. Chaves, J. D. Caldwell, A. Kumar, N. X. Fang, P. Avouris, T. F. Heinz, F. Guinea, L. Martin-Moreno, and F. Koppens, Nat. Mater. **16**, 182 (2017).

[4] H. Raether, *Surface Plasmons on Smooth and Rough Surfaces and on Gratings* (Springer-Verlag, Berlin, 1988).

[5] J. A. Schuller, E. S. Barnard, W. Cai, Y. C. Jun, J. S. White, and M. L. Brongersma, Nat. Mater. **9**, 193 (2010).

[6] A. Liebsch, *Electronic Excitations at Metal Surfaces* (Springer, New York, 1997).

[7] S. R. Barman, C. Stampfl, P. Häberle, W. Ibañez, Y. Q. Cai, and K. Horn, Phys. Rev. B **64**, 195410 (2001).

[8] K.-D. Tsuei, E. Plummer, A. Liebsch, E. Pehlke, K. Kempa, and P. Bakshi, Surf. Sci. **247**, 302 (1991).

[9] K. L. Tsakmakidis, O. Hess, R. W. Boyd, and X. Zhang, Science **358**, eaan5196 (2017).

[10] L. Lu, E. Galiffi, K. Ding, T. Dong, X. Ma, and J. B. Pendry, ACS Photonics **7**, 951 (2020).

[11] S. R. Barman, K. Horn, P. Häberle, H. Ishida, and A. Liebsch, Phys. Rev. B **57**, 6662 (1998).

[12] S. R. Barman, C. Biswas, and K. Horn, Phys. Rev. B **69**, 045413 (2004).

[13] A. Liebsch, G. Hincelin, and T. López-Rios, Phys. Rev. B **41**, 10463 (1990).

[14] V. Zielasek, N. Rönitz, M. Henzler, and H. Pfnür, Phys. Rev. Lett. **96**, 196801 (2006).

[15] Y. Yang, D. Zhu, W. Yan, A. Agarwal, M. Zheng, J. D. Joannopoulos, P. Lalanne, T. Christensen, K. K. Berggren, and M. Soljacic, Nature (London) **576**, 248 (2019).

[16] J. Scholl, A. Koh, and J. Dionne, Nature (London) **483**, 421 (2012).

[17] K. J. Savage, M. M. Hawkeye, R. Esteban, A. G. Borisov, J. Aizpurua, and J. J. Baumberg, Nature (London) **491**, 574 (2012).

[18] C. Ciracì, R. T. Hill, J. J. Mock, Y. Urzhumov, A. I. Fernández-Domínguez, S. A. Maier, J. B. Pendry, A. Chilkoti, and D. R. Smith, Science **337**, 1072 (2012).

[19] D. Jin, Q. Hu, D. Neuhauser, F. von Cube, Y. Yang, R. Sachan, T. S. Luk, D. C. Bell, and N. X. Fang, Phys. Rev. Lett. **115**, 193901 (2015).

[20] See Supplemental Material at http://link.aps.org/supplemental/10.1103/PhysRevLett.125.126802 for experimental setup, sample preparation and characterization, estimation of the linewidth, incident angle dependence,

and computational details. It contains Refs. [6,7,13,19, 21–32].

[21] M. Petrović, I. Šrut Rakić, S. Runte, C. Busse, J. T. Sadowski, P. Lazić, I. Pletikosić, Z.-H. Pan, M. Milun, P. Pervan, N. Atodiresei, R. Brako, D. Šokčević, T. Valla, T. Michely, and M. Kralj, Nat. Commun. **4**, 2772 (2013).

[22] N. Ehlen, M. Hell, G. Marini, E. H. Hasdeo, R. Saito, Y. Falke, M. O. Goerbig, G. Di Santo, L. Petaccia, G. Profeta, and A. Gruneis, ACS Nano **14**, 1055 (2020).

[23] P. J. Feibelman, Prog. Surf. Sci. **12**, 287 (1982).

[24] N. Moiseyev, *Non-Hermitian Quantum Mechanics* (Cambridge University Press, New York, 2011).

[25] T. Yasuike, K. Nobusada, and M. Hayashi, Phys. Rev. A **83**, 013201 (2011).

[26] J. Cai, W. Jolie, C. C. Silva, M. Petrović, C. Schlueter, T. Michely, M. Kralj, T.-L. Lee, and C. Busse, Phys. Rev. B **98**, 195443 (2018).

[27] J. Hrbek, Surf. Sci. **164**, 139 (1985).

[28] D. Bauer, F. Ceccherini, A. Macchi, and F. Cornolti, Phys. Rev. A **64**, 063203 (2001).

[29] *Handbook of Optical Constants of Solids*, edited by E. D. Palik (Academic Press, Burlington, 1997).

[30] A. Siokou, F. Ravani, S. Karakalos, O. Frank, M. Kalbac, and C. Galiotis, Appl. Surf. Sci. **257**, 9785 (2011).

[31] A. Sumiyoshi, H. Hyodo, Y. Sato, M. Terauchi, and K. Kimura, Solid State Sci. **47**, 68 (2015).

[32] T. Yasuike and K. Nobusada, Phys. Rev. B **84**, 245408 (2011).

[33] K. Watanabe, Y. Matsumoto, T. Yasuike, and K. Nobusada, J. Phys. Chem. A **115**, 9528 (2011).

[34] D. Ino, K. Watanabe, N. Takagi, and Y. Matsumoto, J. Phys. Chem. B **109**, 18018 (2005).

[35] R. van Gastel, A. T. N'Diaye, D. Wall, J. Coraux, C. Busse, N. M. Buckanie, F.-J. Meyer zu Heringdorf, M. Horn von Hoegen, T. Michely, and B. Poelsema, Appl. Phys. Lett. **95**, 121901 (2009).

[36] M. Liu, Y. Li, P. Chen, J. Sun, D. Ma, Q. Li, T. Gao, Y. Gao, Z. Cheng, X. Qiu, Y. Fang, Y. Zhang, and Z. Liu, Nano Lett. **14**, 6342 (2014).

[37] J. L. McChesney, A. Bostwick, T. Ohta, T. Seyller, K. Horn, J. González, and E. Rotenberg, Phys. Rev. Lett. **104**, 136803 (2010).

[38] W. H. Weber and G. W. Ford, Opt. Lett. **6**, 122 (1981).

[39] M. Meier and A. Wokaun, Opt. Lett. **8**, 581 (1983).

[40] A. Kubo, N. Pontius, and H. Petek, Nano Lett. **7**, 470 (2007).

[41] M. Dąbrowski, Y. Dai, and H. Petek, Chem. Rev. **120**, 6247 (2020).